Kinetic and structural assessment of the reduction of human 2-Cys Peroxiredoxins by Thioredoxins

Sebastián F. Villar[1,2], Laura Corrales-González[1], Belén Márquez de los Santos[1,3], Joaquín Dalla Rizza[1*], Ari Zeida[2,4], Ana Denicola[1,2] and Gerardo Ferrer-Sueta[1,2]

[1]Laboratorio de Fisicoquímica Biológica, Instituto de Química Biológica, Facultad de Ciencias; [2]Centro de Investigaciones Biomédicas (CEINBIO), [3]Área Inmunología, Departamento de Biociencias, Facultad de Química and [4]Departamento de Bioquímica, Facultad de Medicina, Universidad de la República, Montevideo, Uruguay.

Current address: * Protein Crystallography Unit, Institut Pasteur de Montevideo, Montevideo, Uruguay

Corresponding author contact details: Gerardo Ferrer-Sueta. Laboratorio de Fisicoquímica Biológica. Facultad de Ciencias. Iguá 4225. Montevideo 11400. Uruguay. Phone (598) 2525 8618 Int 213. Email: gferrer@fcien.edu.uy (GFS)

Running title: Reduction of human Prx by Trx

Abbreviations: Prx Peroxiredoxin; Trx Thioredoxin; C_N, nucleophilic cysteine of a Trx; k_{cat}, turnover number; TCEP, tris(2-carboxyethyl)phosphine; LP320, 320 nm long pass filter: U360, 360 nm bandpass filter; TMA buffer, tris-MES-acietic acid buffer; pe, prior equilibrium approximation; ss, steady state approximation; 4-DTDPy,

Keywords: Peroxiredoxin, thioredoxin, catalytic cycle, reaction mechanism, hydrogen peroxide, redox signaling

Conflict of Interest (none to declare),

Abstract

We have studied the reduction reactions of two cytosolic human peroxiredoxins (Prx) in their disulfide form by three thioredoxins (Trx, two human and one bacterial), with the aim of better understanding the rate and mechanism of those reactions, and their relevance in the context of the catalytic cycle of Prx. We have developed a new methodology based on stopped-flow and intrinsic fluorescence to study the bimolecular reactions and found rate constants in the range of

10^5 to 10^6 M^{-1} s^{-1} in all cases showing that there is no marked kinetic preference for the expected Trx partner. By combining experimental findings and molecular dynamics studies, we found that the reactivity of the nucleophilic cysteine (C_N) in the Trx is greatly affected by the formation of the Prx-Trx complex. The protein-protein interaction forces the C_N thiolate into an unfavorable hydrophobic microenvironment that reduces its hydration and results in a remarkable acceleration of the thiol-disulfide exchange reactions by more than three orders of magnitude, and also produces a measurable shift in the pK_a of the C_N.

Introduction

Peroxiredoxins are a family of thiol peroxidases remarkable in terms of their abundance, ubiquity, and diversity. They also have some kinetic aspects in their catalytic cycle that deserve attention and make them unique. In the first decade after the report of Prx as peroxidases, some researchers characterized them as limited in comparison to other peroxidases [1, 2], whereas others found them to be extremely fast [3-5]. Paradoxically, both opinions were correct. In terms of their reaction with H_2O_2 and other peroxides, some Prx are among the fastest reactants, with rate constants (k_{H2O2}) close to the diffusion control limit [4-7]. However, when the whole catalytic cycle is considered, for instance by measuring their turnover number (k_{cat}), Prx have moderate to modest values. The most extreme example of this behavior is human Prx2 (Prx2), whose reaction with H_2O_2 is very fast (k_{H2O2} = 1.6 x 10^8 M^{-1} s^{-1} [6]), but its catalytic cycle is rather slow ($k_{cat} \leq 0.2$ s^{-1}).

The standard catalytic cycle of Prx, particularly those that use two Cys residues for catalysis (2-Cys Prx), consists of three reactions; namely, oxidation by a peroxide substrate (ROOH, Reaction 1, Fig. 1), condensation of the two catalytic cysteines to form a disulfide (Reaction 2, Fig. 1) and reduction of the disulfide by an external reductant (Reactions 3a – 3d, Fig. 1). The oxidation reaction has received the most attention, particularly since realizing that Prx are among the fastest known reductants of H_2O_2 [3, 4, 8]. Interest in the resolution reaction, i.e. the condensation between the sulfenic acid formed in the peroxidatic cysteine (C_P) and the resolving cysteine (C_R) thiol, has increased lately, once it was found that it can be very slow and provide an internal brake of the catalytic consumption of ROOH [6, 7].

The reduction reaction, typically carried out by a thioredoxin (Trx) or similar thiol-disulfide oxidoreductase, has been studied less often. A few works appear in the literature detailing the bimolecular reaction between a Prx and its expected redox partner [5, 7, 9-11]. Among the reactions in the catalytic cycle, the reduction process is the only one requiring a protein-protein interaction and, as such, more complexity can be anticipated. Also, it is not just one chemical reaction but a sequence of two thiol-disulfide exchange steps accompanied by several conformational and association-dissociation changes. In summary, the reduction process is not simple, but a series of interactions, chemical steps and involves changes in tertiary (and perhaps quaternary) structure. A summary of the canonic catalytic cycle of 2-Cys Prx is presented in Fig.

1, with emphasis in the individual reactions, protein-protein associations, and changes in tertiary structure (FF, fully-folded and LU, locally-unfolded states of Prx).

Why is it important to know in detail the catalytic cycle of Prx and in particular the reduction reaction? Beyond mere curiosity, an in-depth knowledge of the kinetics of each step provides a solid starting point to predict which one of the three Prx intermediates may be prevalent in a given situation of H_2O_2 formation and reductant supply. Additionally, Prx disulfide, the reactant in Reaction 3, may be one redox relayer involved in signaling, most likely via a thiol-disulfide reaction. Thus knowing how protein-protein interactions accelerate a similar reaction with Trx may provide clues to orient the search of surface characteristics in the redox partners of Prx.

On the question of the catalytic cycle and the rate limiting step, since the oxidation reaction (Reaction 1 in Fig. 1) has usually the largest rate constant, resolution (Reaction 2) and reduction (Reactions 3a-d) are candidates to be rate-limiting. In human Prx2, step 2 is a prime suspect given its very low rate constant (k_2 = 0.2 s^{-1} [6]). In other 2-Cys Prx the case is not that clear cut, but it is needed to understand how some 2-Cys Prx can act as redox relays from H_2O_2 to signaling partners [12-14]. The rate-limiting step implies that the reactant species in that step accumulate in a situation of sustained cycling. If resolution is rate-limiting, the sulfenic acid form accumulates, whereas if reduction is rate limiting the disulfide is the accumulated form. Since sulfenic acids and disulfides have markedly different reactivities, and their lifetime may be different between different Prx, knowing the rate of reduction is another piece of information needed to understand how each Prx may act as a hub of redox relays.

Each of the three Prx intermediates in the catalytic cycle (Prx-SH, Prx-SOH, $Prx2S_2$) may be involved in side-reactions, in particular, the oxidized forms of sulfenic acid and disulfide have been implicated in reactions leading to redox signaling. The rationale is that H_2O_2 as an oxidant lacks specificity, and its reactions are very slow except for those with peroxidases. Instead, Prx (as sulfenic acid or disulfide) may be recognized by specific targets through protein-protein interactions and act as a proxy oxidant [15]. In such a scenario Prx would have the role of Prx sensor (thanks to their extremely fast Reaction 1) and as a hub, receiving electrons from several targets other than Trx.

Thiol-disulfide reactions are slow in the absence of catalysis, and their rate constants can be predicted for low molecular weight species, the only data needed are pH, the pK_a of the thiols involved, and the empiric equation for thiol-disulfide exchange determined by Szajewski et al [16]. Using the literature pK_a values of Prx2, (4.8 C_P and 8.5 C_R [6]) and the nucleophilic cysteine (C_N) of human Trx1 (*Hs*Trx1) (6.3 [17]), a rate constant for the initial reaction can be estimated as 85 M^{-1} s^{-1} at pH 7. Values in the literature for reduction of Prx by Trx, particularly in pairs of the same species and subcellular compartment range from 8.9×10^4 M^{-1} s^{-1} (*E. coli* TPx reduced by *E. coli* Trx [9]) to 2.3×10^7 M^{-1} s^{-1} (*S. typhimurium* AhpC reduced by the Trx domain of *S. typhimurium* AhpF [7]). There is an evident acceleration of the thiol-disulfide exchange by the protein-protein interactions and it will be interesting to understand how it works, not only to better understand the detailed mechanism of Prx catalysis, but also because

Prx disulfide may well be involved in redox relays leading to signaling events [18]. Those redox relays involving Prx disulfide would also need to have accelerated thiol-disulfide exchange reactions to be competitive in the cellular redox landscape of thiols and disulfides.

In this work we approach the reduction of two human cytosolic peroxiredoxins with the aim of assessing their reduction kinetics and delving into the protein-protein interaction and how they accelerate the reactions. We also discuss the potential involvement of changes in tertiary and quaternary structure into the kinetics of the overall catalytic cycle.

Results and discussion

Reduction of Prx1 and Prx2 with TCEP

Reduction of Prx by TCEP is an unspecific reaction and was measured to ascertain that there is no difference in "reducibility" between Prx1 and Prx2, also, the rate constants were used in the design of later experiments. Both Prx show a small increase in fluorescence upon reduction, followed by a long linear descent (similar descents in fluorescence were observed in many experiments and are attributed to a slow photobleaching of tryptophan). The rate constant of the ascent in fluorescence depends linearly on the concentration of TCEP and the second order rate constants obtained are similar and quite slow: Prx1 (3.66 M^{-1} s^{-1}) and Prx2 (6.25 M^{-1} s^{-1}).

Reduction of Prx2 by Trx

After numerous unsuccessful attempts at trying to monitor the reaction by total tryptophan fluorescence upon mixing Prx and Trx under pseudo first order conditions, we turned to the method described in the Materials and Methods section as rate-limiting approach. Briefly, it consists in starting all three reactions in the catalytic cycle upon mixing and letting them be seen only if they become rate limiting, bearing in mind that the most significant changes in fluorescence arise from the formation and consumption of the sulfenic acid form. For Prx2, the reaction is easier to set up. Starting with [H_2O_2] = 1 μM, the oxidation (Reaction 1) will have a pseudo-first order rate constant ≥100 s^{-1}, whereas the resolution (Reaction 2) is only 0.2 s^{-1}. Therefore, any concentrations of Prx and Trx yielding a pseudo-first order rate constant 100 > k_3> 0.2 s^{-1} will be simultaneously rate limiting in the formation of the sulfenic acid, and faster than its consumption. Thus, the change in fluorescence will be observable. Based on previous reports, rate constants of Reaction 3 involving mammalian Prx are in the range 10^5 – 10^6 M^{-1} s^{-1}, so we chose concentrations in the low micromolar range with $Prx2S_2$ in excess over $Trx(SH)_2$.

The results are shown in Fig. 2. Time courses display the typical descent and then ascent in fluorescence seen upon formation and consumption of Prx(SOH)SH, followed by a linear decrease in fluorescence that is seen even in the absence of Trx. The kinetic parameters were obtained by fitting Equation 2 to the time courses, the rate constants of the descents (k_{dn}) were plotted as a function of [$PrxS_2$] and the slope of the linear regression yields the second-order rate constants that appear in Table 1.

Reduction of Prx1 by Trx

Applying the kinetic considerations of the rate-limiting method to Prx1, the resolution being so much faster (12.9 s^{-1}) than that of Prx2 constitutes a hurdle. If we assume a rate constant in the order of 4×10^5 M^{-1} s^{-1}, the concentration of Trx needed to make the pseudo-first order rate constant of Reaction 3 greater than 12.9 s^{-1} is 32 μM, thus we made the experiments with $Trx(SH)_2$ in excess and in the range from 5 to 190 μM, with 0.5 – 5 μM $Prx1S_2$ and at least 10 μM H_2O_2. The time courses show an unexpected small increase in fluorescence in the first 10 ms followed by a slower and more marked descent, and the final increase in fluorescence is only observed after H_2O_2 is depleted. The kinetic parameters were obtained by fitting Equation 2 to the first 0.2 s of the time courses. The two rate constants obtained, named k_{up} and k_{dn}, were plotted as a function of Trx concentration yielding straight lines in both cases. These results are shown in Fig. 3.

Reaction order and interpretation of kinetic data

When we began studying the reduction reaction of Prx by Trx we only aspired to obtain rate constants, assess rate limiting steps in the catalytic cycle, and hopefully understand differences among various Trx and between Prx1 and Prx2. As usual, the study of the reactions revealed a more complex landscape. Since the total fluorescence approach yielded ambiguous and poorly reproducible results, we opted for a better experimental setup that only reveals those steps that are rate limiting to the formation of sulfenic acid (Reaction 1, Fig. 1). Starting from $PrxS_2$ and up to Prx(SOH)SH, the only process that is first order in both Trx and Prx is Reaction 3a. Reaction 3b may also appear to be first order in both proteins if 3a is reversible and appreciably fast in both directions, following the next scheme [19].

$$Trx(SH)_2 + PrxS_2 \underset{k_{-3a}}{\overset{k_{3a}}{\rightleftharpoons}} Trx(SH)_2{:}PrxS_2 \xrightarrow{k_{3b}} Trx(SH)\text{-}S\text{-}S\text{-}Prx(SH)$$

In those cases, the rate constants of the overall processes from $PrxS_2$ to Trx(SH)–S–S–Prx(SH) (steps 3a and 3b, Fig.1), or k_{3ab} can be approximated as:

$$rate = k_{3ab}^{pe}[PrxS_2] = \frac{k_{3a}k_{3b}[Trx(SH)_2]}{k_{-3a} + k_{3b}}[PrxS_2] \qquad \text{(Equation 6)}$$

Assuming process 3a is a prior equilibrium, or,

$$rate = k_{3ab}^{ss}[PrxS_2] = \frac{k_{3a}k_{3b}[Trx(SH)_2]}{k_{3a}[Trx(SH)_2] + k_{-3a}}[PrxS_2] \qquad \text{(Equation 7)}$$

Assuming the intermediate is in a steady state.

The choice of the approximation depends on the relative values of k_{-3a} and k_{3b}. If $k_{-3a} > k_{3b}$ a prior equilibrium is a better approximation, but if $k_{3a}[Trx(SH)_2] > k_{-3a} + k_{3b}$, a steady state is a better description. Each approximation has a characteristic dependence on the concentration of reagents, k_{3ab}^{pe} depends linearly on $[Trx(SH)_2]$, whereas k_{3ab}^{ss} dependence is hyperbolic with an asymptote value equal to k_{3b}.

The experiments measuring Prx2 reduction seem straightforward, we observed a single process with a descent in fluorescence and linear dependence on [Prx2S_2] (Fig. 2). The second-order rate constants measured in Fig. 2C thus correspond either to k_{3a} or k_{3ab}^{pe}, for the three Trx studied (Table 2). Meanwhile, the rate constants of Fig. 2D are zero order in [Prx2S_2] and coincide in value with the previously determined k_2 [6].

The scenario with the reduction of Prx1 is a bit more complex, perhaps because the reactions had to be performed with significantly higher concentrations of both Trx and Prx. Two processes are apparent, a fast one that produces an upward change fluorescence with a rate constant k_{up} and a slower one that results in the fluorescent descent with a rate constant k_{dn}, consistent with sulfenic acid formation. When human Trx are employed, k_{up} depends linearly with [Trx$(SH)_2$] whereas k_{dn} appears to be independent of [Trx$(SH)_2$]. That would be consistent with k_{up} corresponding to k_{3a}, and k_{dn} corresponding to k_{3ab}^{ss} in which the ascending part of the hyperbola should appear at [Trx$(SH)_2$] below the experimental range, or it could also be k_{3c} or k_{3d}, as both are zero order in [Trx$(SH)_2$], whichever is smaller, and results the rate-limiting step in the reduction process.

In the reaction of Prx1 with *Ec*Trx both k_{up} and k_{dn} depend linearly on [Trx$(SH)_2$], thus, the only possible explanation is that k_{up} is k_{3a} and k_{dn} is k_{3ab}^{pe}. Given that k_{-3a} can be measured from the *y*-intercept of Fig. 3D (red line, y_0 = 58 s^{-1}), k_{3b} can be arithmetically calculated from Equation 6 since we know $k_{3a} = 2.5 \times 10^6$ M^{-1} s^{-1}, and $k_{3ab}^{pe}/[\text{Trx}(SH)_2] = 5.3 \times 10^5$ M^{-1} s^{-1}. Then, substitution in Equation 6 yields a k_{3b} value of approximately 16 s^{-1}. However, the uncertainty on this value is somewhat large, owing to k_{-3a} being an extrapolated value and the combination of the uncertainties of several experimental values.

Reduction of Prx2 by Trx as a function of pH

Since the determination of rate constants was relatively simple in the case of Prx2, we measured them as a function of pH to better understand the protein-protein interactions and their effect on the nucleophilic attack of Trx. The experiments were made in TMA buffer to avoid confounding effects arising from the change in ionic strength and with only one concentration of Trx$(SH)_2$ (0.2 μM) and Prx2S_2 (2 μM) at each pH in the range from 4.5 to 8.5. The apparent rate constants were plotted vs pH and, since the plots were bell-shaped, Equation 4 was used to obtain the values of two pK_a in each case. The results appear in Fig. 4 and Table 2. Surprisingly, neither pK_a coincided with the reported values of any of the Trx tested. Since the reduction reaction is first order in Trx, as seen in Fig. 2, its rate constant should increase upon ionization of the nucleophilic cysteine (C_N), so we took the inflection point of the ascending part of the bell shape as pertaining to the C_N. As our method for measuring the rate constant of reduction by Trx relies on the reaction being slower than the oxidation by peroxide, a control experiment was made measuring the oxidation of Prx2 as a function of pH to ascertain that the rate constant of Reaction 1 is larger than k_{dn} throughout the pH range studied. At any pH in the range from 4.5 to 7.8 k_1 is at least 50-fold larger than k_{dn} (not shown).

Measurement of Trx pK_a

There are multiple reports of pK_a of the nucleophilic cysteine of several Trx in the literature, many of these values are listed in Table 2. The exception seems to be *Hs*Trx2 for which we could not find a pK_a value. Our intention in doing these experiments was to complement the values from the literature with results obtained in our lab under conditions similar to the previously mentioned reactions of reduced Trx with Prx2 disulfide as a function of pH. Of particular importance for this, we measured the pK_a of *Hs*Trx1, *Hs*Trx2 and *Ec*Trx through the change in the rate constant of reaction with an unspecific disulfide, 4-DTDPy, that yields a product that absorbs at 324 nm [24]. The pH profile of this reaction has the expected increase in rate constant with two inflection points for *Hs*Trx1 (pK_{a1} = 6.1 and pK_{a1} = 7.6), or one inflection point *Hs*Trx2 (pK_a = 7.15), and for *Ec*Trx (pK_a = 7.4) (see Table 2). However, the pH profiles are quite different from their counterparts of each Trx with the disulfide of Prx2. In Fig. 4E the pK_a shift is readily observable. Additionally, the pK_a of *Hs*Trx2(SH)$_2$ was measured through the absorbance of the thiolate at 240 nm (not shown).

Reduction and the LU → FF transition

The disulfide bond in oxidized Prx fixes their active site in the locally unfolded (LU) conformation, whereas the fully folded (FF) conformation is required for the fast reduction of H_2O_2. It can be regarded as if Prx had two different active sites, one for Trx in the LU conformation and a different one for hydroperoxides in the FF conformation. The rate of the LU → FF transition in Prx upon reduction is unknown, so we decided to try to measure it and also to see if Trx provided assistance for the conformational change. The experiment was performed in the stopped flow with a sequential mixing setup. In the first step Prx2S$_2$ was mixed with excess reductant (either *Hs*Trx1(SH)$_2$ or TCEP). After a preset ageing time (2 – 40 s) and a second mixing with excess H_2O_2 we measured the rate constant of fluorescent decay (associated to Reaction 1, Fig. 1). In all cases the observed rate constant coincided with that obtained with pre-reduced Prx2 implying that the LU → FF transition is faster than the reduction under the experimental conditions and that if Trx favors the transition, this is not observable under the timeframe of the experiment.

Reduction of Prx in the context of the catalytic cycle

We previously proposed that the resolution reaction can be viewed as a built-in brake that impedes Prx to simply consume all H_2O_2 as catalase would. This means that Prx can sense minute levels of H_2O_2 and transmit the information in a useful way to promote signaling through their oxidized forms of sulfenic acid and disulfide [6]. When that proposal was made, we still lacked the detailed information of the reduction reactions, and now, through this work, we have a more complete set of rate constants that could help us understand the workings of the catalytic cycle. First, we can ask under what circumstances each of the three main steps of the catalytic cycle (namely, oxidation, resolution and reduction) becomes rate limiting. The answer is

straightforward for Prx2, since its resolution reaction is so slow (k_2 = 0.2 s^{-1}) and considering that $k_1^{H_2O_2}$ and $k_3^{Hs\text{Trx1}}$ are relatively fast, concentrations of [H_2O_2] > 1.25 nM and [*Hs*Trx1] > 325 nM are sufficient to make resolution the rate limiting step.

The case of Prx1 is a bit more complex. Resolution is faster (k_2 = 12.9 s^{-1}) and reduction has a rate limiting step that is zero order in *Hs*Trx1 (k_{3b}, k_{3c} or k_{3d}) with a similar rate constant of 15.8 s^{-1}, that makes the reduction step essentially independent of [*Hs*Trx1] and a [H_2O_2] >120 nM would be sufficient to outcompete resolution. But there is another piece of information that needs to be considered, when the catalytic cycle is measured using oxidation of NADPH through *Ec*Trx and *Ec* thioredoxin reductase it appears to have a turnover number between 2 and 4.8 s^{-1} [25, 26]. This surprisingly low k_{cat} must arise from a still nondescript process that further slows down the catalysis. One possible candidate is a change in reactivity associated with the oligomeric state of Prx1, our reduction experiments were made with Prx1 mostly as decamers while NADPH oxidation experiments were made with 500 nM Prx1, mostly in dimeric form [27].

Finally, the LU-FF equilibrium could also be rate limiting, the refolding of the peroxidatic active site in the FF conformation appears, in the case of Prx2, to be independent of the presence of Trx, or to be over in 2 s independently of the used reductant. This supports the notion that the resolving step is the rate limiting process of Prx2 catalytic cycle. However, we did not attempt a similar experiment with Prx1 as it would involve impractical concentrations of TCEP, but since our kinetic methodology relies on a very fast Reaction 1, from the results in Fig. 3D, we can conclude that the refolding process occurs with a rate constant higher than 15 s^{-1}.

Structural insight of the Prx-Trx interaction

To this date, there are no reported structures of complexes between 2-Cys Prx and Trx. There is one structure of Prx2 in its disulfide form [28] whereas the sole available structure of Prx1 has a CHAPS molecule bound to the disulfide and is also a C83S mutant [29]. This motivated us to generate our own models, using protein-protein docking of the complexes between $Prx2S_2$ and *Hs*Trx1, *Hs*Trx2 and *Ec*Trx, in their reduced state. A blind-docking approach didn´t yield satisfying results, since the Trx was placed far from the disulfide of Prx2 and its active site was outside the interaction interphase. Therefore, we decided to guide the docking (using the criterion described in the Materials and Methods section) to obtain a reactive complex, i.e., a complex in which the chemical reaction would likely happen. Then, we ran 500 ns-long MD simulations of each complex to further assess the structural features of the Prx-Trx interaction. As a result of the guided molecular docking protocol the Trx binds the locally unfolded C_R loop of Prx2 on its groove, where the C_N approaches the C_R of the disulfide from the side or from above. The results of the docked complexes, the interacting residues and energy calculation after 500 ns of simulation are presented in Fig. 5.

We identified an amphipathic interaction surface comprising two regions: region 1 is a hydrophobic core involving Trx C_N, the Prx2 disulfide and other non-polar residues; region 2 contains polar interactions in areas surrounding region 1 (Fig. 5A). We estimated the binding

free energy ($\Delta G_{Binding}$) for the three complexes (Fig. 5B) and decomposed it in a per residue basis to identify their importance for the stabilization of the complex (Fig. 5 C).

In region 1, residues W31, P34, M37, C73, M74, P75, G91, A92 (*Hs*Trx1) and V171, P173, A174, G175, W176 (Prx2), surround the disulfide of Prx2 and Trx C_N and define the hydrophobic interaction core. Among these, M74 and C_R stand out as the most stabilizing residues in *Hs*Trx1 and Prx2 respectively (Fig. 5C), and the same was observed with V74 and I75 in *Hs*Trx2 and *Ec*Trx, respectively. Both residues interact through backbone-backbone hydrogen bonds and orient the disulfide towards C_N (Fig. 5D-F). Trx residues within region 1 have the largest contribution to complex stabilization (Fig. 5C). Interestingly, the latter are conserved in canonical Trxs [30].

Region 2 comprises amino acids forming ionic and/or polar interactions with each other, like D60, D61, N93 on *Hs*Trx1 and K92, Y164, H168, K177 on Prx2. In this case, D60 and D61 interact with K92 and K177 forming transient saline bridges throughout the simulation, which endowed the complex with an important electrostatic complementarity. On the opposing side, N93 has hydrogen bond interactions with H168 and Y164. Nevertheless, region 2 varies in the complexes with *Hs*Trx2 and *Ec*Trx, and other ionic and polar interactions were observed, namely, R41 (*Hs*Trx2) with E167 (Prx2) and R72 (*Ec*Trx) with D151 (Prx2) (Fig. 5E and 5F, respectively).

The C_N thiolate induces conformational changes and destabilizes the Prx-Trx complex

The thiolate of Trx C_N (C_NS^-) is the reactive species that will attack $PrxS_2$ and generate the Prx-Trx mixed disulfide intermediate (Fig. 1 Reaction 3b). Therefore, C_NS^- needs to be inside the complex for the reaction to happen. To assess the effect of C_N protonation state, we ran simulations of our three Trx-$Prx2S_2$ complexes with C_N as a thiolate. We observed a systematic increase in the $\Delta G_{Binding}$ of all the complexes when compared to the results obtained with the thiol form, meaning that C_NS^- has a destabilizing effect on the Prx-Trx interaction (Fig. 6A, 6B and 6C). This is further confirmed by the decomposition of the $\Delta G_{Binding}$, where C_NS^- (C32) increases the binding energy by more than 5 kcal/mol. Furthermore, we saw that C_NS^- disrupted nearby interactions in region 1 (i.e., W31, P34, W176) and had a pronounced effect on farther residues in region 2 (i.e., D60, D61, K92, K177). When we took a closer look, we noted that C_NS^- promote W31 to flip out of region 1 to region 2 and distort the interactions of D60 and D61 with K92 and K177. The conformational change of W31 from a closed to an open state could be described by the change in the dihedral formed by the carbonyl, α, β and γ carbon atoms (Fig. 6E). Dihedral values around -50° represent the closed conformation, which is the main region that W31 explores with the C_N as a thiol. Whereas in the presence of C_NS^-, W31 explores different dihedral values, namely 60° (open conformation), -50° and -80° (Fig. 6C). Interestingly, the values of the dihedral match the $\Delta G_{Binding}$ profile throughout the simulation (Fig. 6D) and we saw that the closed conformation correlates with lower binding energies, whereas the open one coincides with higher binding energies (Figs. 6D and 6F).

Complex formation decreases the exposure of C_NS^- to the solvent

The negative charge around C_NS^- in the hydrophobic environment of region 1 not only produces an increase of the $\Delta G_{Binding}$, but also introduces water molecules to the interaction surface. This can be seen in Fig. 7 when the thiol and thiolate of *Hs*Trx1 C_N are compared. Additionally, we simulated *Hs*Trx1 alone in its thiolate state, to compare the solvation of C_NS^- in the absence or presence of the protein interface. As expected, the C_NS^- is less solvated when *Hs*Trx1 is complexed with Prx2, thus, the reactivity of C_NS^- is enhanced by the protein interaction.

Protein-protein interaction and the activation of C_N of Trx

In the introduction we calculated a rate constant for the initial attack of *Hs*Trx1 C_N on the disulfide of Prx2 as 85 M^{-1} s^{-1}, yet the experiments show a rate constant that is more than three orders of magnitude faster (Table 1). The increased reactivity stems from the protein-protein interaction and additional experimental and computational data helps understand the causes. The first striking difference we observed is the decrease in pK_a values of the C_N. Measured through the oxidation by an unspecific disulfide such as 4-DTDPy all three Trx show pK_a values consistent with those in the literature obtained by spectroscopic or unspecific reactions (Table 2). When measured through the oxidation by Prx2 all three Trx showed a $\Delta pK_a \approx -1$. Although this decrease in pK_a provides an increase in the relative concentration of the thiolate (the reacting species of C_N), its contribution is negligible. For instance, at pH = 7.4 *Hs*Trx1 C_N is 95% ionized as per the pK_a = 6.1 of the free protein, whereas the interaction with Prx2 lowers the pK_a to 5.3 yielding 99% ionization of the C_N at the same pH. This 4% difference would most likely be lost into the dispersion of experimental results. The change in pK_a does not explain the change in reactivity but reveals that the interaction results in a significant modification of the C_N environment.

The description of the Trx-Prx interaction surface obtained from the docking and MD simulations reveals several potential contributors to the enhanced nucleophilicity of the C_N. The residues surrounding the C_N are mostly uncharged and nonpolar, in Fig. 5 we can see that the neighbors of the C_N sulfur in a 5 Å radius are G33, P34, C34 and M74 from *Hs*Trx1 and from Prx2 the disulfide C51-C172, V171, P173 and A174. This yields a hydrophobic environment that increases the rate of thiol-disulfide exchange reactions [31]. In line with this observation, the solvation of C_N thiolate decreases in the Trx-Prx complex relative to the free Trx (Fig. 7A). The radial distribution of water molecules is diminished by the formation of the complex (Fig. 7B) and solvation by a polar and hydrogen-bonding solvent such as water is a great way to attenuate the nucleophilic reactivity of thiolates [32].

It was interesting to see that the changes in the dihedral of W31 induced by the negative charge of C_NS^- allowed the entry of water molecules to the reactive region (Prx2 disulfide and C_NS^-) and correlate with the $\Delta G_{Binding}$ of the complex (Fig. 6D and 6F). The movement of W31 from a closed to an open conformation releases the steric hindrance produced by W31 on C_N (Fig. 7C).

The final contributor to the enhanced reactivity is revealed by the energetics of the interaction, Fig. 5C shows the $\Delta G_{Binding}$ contribution of each amino acid residue involved in the Trx-Prx interaction surface. Remarkably, all residues in the interface stabilize the interaction except for C_N as a thiolate (Fig. 6A, 6B and 6C), alternatively it can be construed that all involved residues anchor the C_N thiolate in an unfavorable position that destabilizes it, yielding an enhancement of its reactivity.

Concluding remarks and future developments

On finishing this article, several details and questions still need to be addressed to fully understand the processes associated with the reduction of the Prx within the canonic catalytic cycle and especially when the Prx is reduced by alternative reductants involved in redox relays. For instance, understanding the energetic details of the activation of the C_N would involve a quantum mechanical approach. There is also the question of how much the oligomeric state of the Prx affects the interactions and reactions with Trx. The proposed interaction of Prx either as a sulfenic acid or as a disulfide with potential alternative reductants acting as redox relays [14] opens a plethora of unknowns, such as: What are the Cys residues in the target proteins? How are they activated? Additionally, kinetic restrictions indicate that a preexisting complex between the reduced Prx and its target reductant needs to exist in order to compete with the reduction by Trx [33]. And finally, there is the question of existing scaffold proteins that potentially connect Prx with their target reductants [12]. With the number of potential targets of Prx redox relays being counted by the hundreds [34] there is still much study to be done to understand the reduction of Prx in catalysis and signaling.

Some of the most relevant findings of this study, beyond the numerical parameters of the rate constants, are the existence of a hydrophobic interaction interface surrounding the reacting thiolate and disulfide, which partially excludes water around the reactants. Also, the energetics of the binding is favored by about twenty amino acids in both Trx and Prx but destabilized by C_N thiolate. Overall, desolvation and immersion in a more hydrophobic environment causes an increase in nucleophilicity that may explain the three orders of magnitude increase of the measured rate constants compared with those calculated in aqueous solution. Extrapolating to alternative redox partners involved in redox relays with Prx disulfides, one may look for one exposed cysteine residue surrounded by a hydrophobic patch.

Materials and Methods

General procedures

Two main buffer systems were used throughout this study, one contains 50 mM sodium phosphate, 150 mM NaCl, 0.1 mM dtpa, pH 7.4, is referred to as phosphate buffer. The second system contains 30 mM tris, 15 mM MES, 15 mM acetic acid, 120 mM NaCl and 0.1 mM dtpa, it is used as a wide range pH buffer and is referred to as TMA buffer.

To obtain the reduced form of the proteins, they were treated with either 10 mM DTT or 10 mM tris(2-carboxyethyl)phosphine (TCEP) for 30 min at room temperature, and the excess reductant was removed using a PD10 column. Protein concentration was determined by their absorbance at 280 nm using the following extinction coefficients (calculated from their sequences using the ProtParam tool): Prx1 (Uniprot Q06830), 18500 M^{-1} cm^{-1}; Prx2(Uniprot P32119), 21500 M^{-1} cm^{-1}; *Hs*Trx1 (Uniprot P10599), 7000 M^{-1} cm^{-1}; *Hs*Trx2 (Uniprot Q99757), 7000 M^{-1} cm^{-1}; *Ec*Trx (Uniprot P0AA25), 14000 M^{-1} cm^{-1}. Thiol content was measured by reduction of 4,4'- dipyridyl disulfide (4-DTDPy) and the absorbance of the products at 324 nm (ε = 21400 M^{-1} cm^{-1}) [35].

Proteins

Recombinant proteins were expressed and purified as previously reported, Prx1 [36], Prx2 [37], *Ec*Trx [38], *Hs*Trx1 [4], *Hs*Trx2 [5].

Prx reduction by TCEP

The reaction of 0.5 μM $Prx1S_2$ or Prx2 S_2 with excess TCEP (5 – 35 mM) was monitored by tryptophan fluorescence in pH 7.4 phosphate buffer. TCEP hydrochloride was previously neutralized with 4 equivalents of tris to keep the same pH in all conditions. Time courses showed a small amplitude exponential followed by a linear descent. Equation 1 was used to obtain the pseudo first order rate constants.

$$y = \text{Amp} \times \exp(-k_{obs} \times x) + b \times x + C \qquad \text{(Eq. 1)}$$

Where y is the fluorescence emission, Amp is the amplitude of the exponential, k_{obs} is the pseudo first order rate constant, b is the slope of the linear function, x is time, and C is the value of the exponential function at infinite time.

The values of k_{obs} were plotted vs [TCEP] to obtain the second-order rate constants.

Prx reduction by thioredoxins

Total fluorescence approach

Several attempts were made to monitor the reduction of both Prx1 and Prx2 by different Trx (*Hs*Trx1, *Hs*Trx2, *Ec*Trx) by following the total emission of the sample after mixing in the stopped flow. The experiments were designed to yield reduced Prx and the protein should stay reduced, otherwise the oxidation and resolution processes would be superimposed to the reduction. Since adventitious H_2O_2 has been reported to affect the results of experiments involving reduced Prx [3], all buffer solutions (either phosphate or TMA) were treated with immobilized catalase (Sigma C9284) to remove adventitious H_2O_2 and then filtered before use. The reaction mixtures consisted in Trx (reduced with 10 mM DTT and gel filtered using a PD10 column) and Prx (oxidized with H_2O_2 equimolar and desalted using a PD10 column) in any of three possible concentration relations: 0.5 μM Prx with Trx with at least a tenfold excess; 0.5 μM Trx with Prx with at least a tenfold excess; or a constant ratio of concentrations with 10 [Prx] = [Trx]. The results yielded poor reproducibility and ambiguous dependencies on the excess reactant, in our hands, even the smallest concentration of adventitious H_2O_2 resulted in the

appearance of additional phases in the change of fluorescence. A detailed report of this approach and results obtained with Prx1 was published elsewhere [39].

Rate-limiting approach

The reaction was carried in the stopped flow, monitoring tryptophan fluorescence with 280 nm excitation and emission using either a 320 nm long pass filter (LP320) or a 360 nm bandpass filter (U360). The equipment mixed one syringe containing Prx2 as a disulfide (0 – 6 μM after mixing) and H_2O_2 (1 μM after mixing) with the other syringe containing reduced thioredoxin (0.2 μM after mixing). Both solutions were in phosphate buffer. Under these conditions Prx undergoes the following series of reactions:

- $PrxS_2$ reacts with $Trx(SH)_2$ to yield $Prx(SH)_2$. (Reactions 3a to 3d in Fig. 1)
- $Prx(SH)_2$ reacts with H_2O_2 to yield Prx(SOH)(SH). (Reaction 1 in Fig. 1)
- Prx(SOH)(SH) reacts internally to form $PrxS_2$. (Reaction 2 in Fig. 1)

This method takes advantage of several favorable conditions of Prx2 kinetics and fluorescence: first, Reaction 1 is extremely fast, with an expected apparent rate constant ≤ 100 s^{-1} with 1 μM H_2O_2; second, Reaction 2 is quite slow, with an expected apparent rate constant of 0.2 s^{-1} under the experimental conditions; and finally, most of the change in fluorescent emission happens in Reaction 1 (decrease) or Reaction 2 (increase), since $PrxS_2$ and $Prx(SH)_2$ have very similar spectra and quantum yields, as a result, the only detectable changes in fluorescence happen during the formation and consumption of the sulfenic acid. Under the conditions of the assay the contribution of Trx to the fluorescence change is minimal, *Hs* Trx1 and *Hs* Trx2 have very low quantum yields and *Ec* Trx has a fluorescence change that goes in the same direction as the change in Prx.

The fluorescence time course of the reactions has the familiar biphasic pattern observed in the oxidation of Prx2 and other proteins of the Prx1 family [6, 7, 26, 40, 41]. However, since Reaction 1 is much faster than Reaction 3, what is observed as the decrease in fluorescence associated with oxidation to sulfenic acid is actually the rate-limiting formation of $Prx(SH)_2$, resulting in an apparent rate constant of the downward exponential much slower than the expected ≤100 s^{-1} of Reaction 1, as will be presented in the results section.

To study the reduction reaction as a function of pH, TMA buffer was used, this buffer can be used in the 4 to 8.5 pH range and its ionic strength is nearly constant [42]. The kinetic parameters were obtained by fitting a sum of two exponential and one linear function, as in Equation 2 to the time courses.

$$y = \text{Amp1} \times \exp(-k^1_{obs} \times x) + \text{Amp2} \times \exp(-k^2_{obs} \times x) + b \times x + C \qquad \text{(Equation 2)}$$

Where y is the fluorescence emission, Amp 1 and k^1_{obs} , and Amp2 and k^2_{obs} are the amplitude and rate constant of each exponential, b is the slope of the linear portion and x is time.

This approach was tried for Prx1 in a limited set of experiments using the Trx as reactant in excess. Reaction 2 is much faster in the case of Prx1 (12.9 s^{-1} [6]), therefore, large concentrations

of Trx were needed to make the buildup of sulfenic acid (via Reactions 3 and 1) faster than its consumption via Reaction 3. Based on the results obtained for Prx2 and assuming similar rate constants with Trx, the experiments were made by mixing the contents of one syringe containing $Prx1S_2$ (5 μM after mixing) and excess H_2O_2; the other syringe contained reduced thioredoxin (40 – 150 μM after mixing). After the initial attempts we found that smaller concentrations yielded useful results, so $Prx1S_2$ was 0.5 μM and *Hs*Trx1 ≥ 5 μM in the final assays. Both solutions were in TMA buffer, pH 7.1 - 7.2. The kinetic parameters were obtained using Equation 2.

Reduction and the LU → FF conformational transition

To explore the potential influence of the reductant on the kinetics of the LU → FF conformational transition we performed experiments with the stopped flow in sequential mode. After the first mix 0.8 μM $Prx2S_2$ is left to react with either 1 μM *Hs*Trx1$(SH)_2$ or 65 mM TCEP during a preset aging time ranging from 2 – 40 seconds, then the resulting mixture is mixed with 1 μM H_2O_2 and the rate constant of oxidation (Reaction 1 in Fig. 1) is measured. The concentrations of reductants were chosen so the reduction occurs with similar rates in both cases and the reduction reaction has a $t_{½} < 2$ s.

Thioredoxin pK_a

The pK_a values of *Hs*Trx1, *Hs*Trx2 and *Ec*Trx were measured and compared to values obtained from the literature.

*Hs*Trx1, *Hs*Trx2 and *Ec*Trx pK_a were determined by the variation of the rate constant of reduction of 4-DTDPy by Trx$(SH)_2$. Briefly, 2.5 μM Trx$(SH)_2$ was mixed with a fixed excess 4-DTDPy in TMA buffer pH 6 – 7.9, the reaction was monitored through absorbance at 324 nm and the resulting time courses were fitted to a single exponential function as in equation 3.

$$y = \text{Amp} \times \exp(-k_{obs} \times x) + C \qquad \text{(Equation 3)}$$

Where y is the absorbance at 324 nm, Amp is the Δabsorbance, x is time and C is the absorbance at the end of the reaction.

The values of k_{obs} were plotted as a function of pH and fitted to a two pK_a function as in Equation 4 in the case of *Hs*Trx1.

$$y = \frac{a_1}{1+\frac{K_{a1}}{[H^+]}+\frac{K_{a1}K_{a2}}{[H^+]^2}} + \frac{a_2}{\frac{[H^+]}{K_{a1}}+1+\frac{K_{a2}}{[H^+]}} + \frac{a_3}{\frac{[H^+]^2}{K_{a1}K_{a2}}+\frac{[H^+]}{K_{a2}}+1} \qquad \text{(Equation 4)}$$

Where y is k_{obs}; a_1, a_2 and a_3 are the apparent rate constant values of the diprotic, monoprotic and aprotic species involved in the two acid-base equilibria, and K_{a1} and K_{a2} are the two ionization constants.

In the case of *Hs*Trx2 and *Ec*Trx, a single pK_a sigmoidal function was used for fitting, as in Equation 5.

$$y = A\frac{[H^+]+K_a}{[H^+]} + B\frac{[H^+]+K_a}{K_a} \qquad \text{(Equation 5)}$$

Where y is k_{obs}, A and B are the extrapolated values of rate constant at extreme acidic and extreme basic pH, respectively.

*Hs*Trx2 pK_a was also determined by the change of thiolate absorbance measured at 240 nm as a function of pH, normalized by absorbance at 280 nm as previously reported [43]. The results between pH 6 and 9 show two inflection points therefore the pK_as were fitted using Equation 4.

Computational Methods

Protein-Protein Docking

Haddock 2.4 [44, 45] was used in order to generate the Prx2-Trx complexes. The input structures for disulfide Prx2 (5IJT) and reduced *Hs*Trx1 (1TRV), *Hs*Trx2 (1UVZ) and *Ec*Trx (1XOB) were collected from the PDB database. The docking protocol consisted in the generation of 5000 structures for rigid body docking followed by ten trials of rigid body energy minimization, then 400 structures were generated for the semi-flexible refinement and no final water refinement was performed. Additionally, several distance restraints were added as "unambiguous restraints", namely between the sulfur atoms of Prx2 C172 and Trx C32 (4 ± 0.5 Å) and their alpha carbons (7 ± 0.8 Å), and between the alpha carbons of Prx2 C172 and M74 (*Hs*Trx1), V74 (*Hs*Trx2), and I75 (*Ec*Trx) (5 ± 0.4 Å). We applied these restraints to guide the docking based on the following criteria:

i. The nucleophilic cysteine (C32, C_N) of Trx and the disulfide of Prx2 need to be close to each other in the reactive complex and the nucleophilic attack is on the sulfur atom of resolving cysteine (C_R, C_{172}) of Prx).
ii. Structural information regarding complexes of Trx and non-Prx substrates, show that the Trx residue at position 74 places the disulfide near the C_N on the binding groove [46-49].
iii. Before docking the whole Prx2S_2 to the Trx, we performed a peptide-docking of a C-term peptide of Prx2 (His168 to Pro178) as a quick descriptor of the substrate's positioning on Trx.

The selection of the best complexes for the molecular dynamics simulations was made based on the HADDOCK score, Trx C_N orientation towards the disulfide of Prx2 and overall electrostatic complementarity.

Molecular Dynamics Simulations

Reduced *Hs*Trx1 and Prx2-Trx complexes were subjected to classical molecular dynamics (MD) in explicit solvent. We performed two sets of simulations, one with the nucleophilic cysteine of Trx as thiol and the other as thiolate (C_NS^-). Systems were immersed in an octahedral box of TIP3P waters, using a 14 Å minimal distance from the complex surface to the end of the box. Protein parameters were generated with the Amber force field parm14SB [50], and newly

developed parameters were used in the case of Trx C_NS^- [51]. All simulations were performed with the *pmemd* module of the AMBER18 [52] package under periodic boundary conditions with a 10 Å cutoff and particle mesh Ewald summation method for treating the electrostatic interactions. The hydrogen bond lengths were kept at their equilibrium distance by using the SHAKE algorithm. Temperature and pressure were maintained with a Langevin thermostat and barostat respectively, as implemented in the AMBER18 program. Each system was minimized in 1000 steps (10 with steepest descent and the rest with conjugate gradient). They were then heated from 0 to 300 K for 20 ps at constant pressure (with a Berendsen thermostat) that later was equilibrated at 1 bar. Finally, 500-ns-long production MD simulations were performed for each system, with a distance restraint of 5 Å between the sulfur atoms of the nucleophilic cysteines of Trx and Cys172 of Prx2. The external potential on the mentioned distance was null between 0 and 5 Å and increased parabolically from 5 Å onward, acting as a "wall-like" potential with a constant value of 100 kcal/mol.

Binding free energy ($\Delta G_{Binding}$) estimations were obtained within the MM-GBSA scheme [53]. For each estimation and decomposition, sets of 1000 simulation frames were used.

Author contributions

Conceptualization, SFV, AZ, AD, GFS; Investigation (wet and in silico measurements): SFV, LCG, BMS, JDR, AZ, GFS; Writing—original draft preparation: SFV, AZ, AD, GFS; Writing—review and editing: SFV, BMS, JDR, AZ, AD, GFS; Funding acquisition: AD, GFS. All authors have read and agreed to the published version of the manuscript.

Acknowledgements

We are grateful for funding from Comisión Sectorial de Investigación Científica, Universidad de la República (CSIC Grupos 2018 to AD), Agencia Nacional de Investigación e Innovación (ANII FCE 2019-155969 to GFS). SFV is supported by a Doctoral Scholarship from ANII, Uruguay, Universidad de la República (CSIC) and PEDECIBA. The simulations presented in this paper were carried out using ClusterUY (site: https://cluster.uy).

References

1. Montemartini, M., Kalisz, H. M., Hecht, H. J., Steinert, P. & Flohe, L. (1999) Activation of active-site cysteine residues in the peroxiredoxin-type tryparedoxin peroxidase of Crithidia fasciculata, *Eur J Biochem.* **264**, 516-24.
2. Flohe, L., Budde, H., Bruns, K., Castro, H., Clos, J., Hofmann, B., Kansal-Kalavar, S., Krumme, D., Menge, U., Plank-Schumacher, K., Sztajer, H., Wissing, J., Wylegalla, C. & Hecht, H. J. (2002) Tryparedoxin peroxidase of Leishmania donovani: molecular cloning, heterologous expression, specificity, and catalytic mechanism, *Arch Biochem Biophys.* **397**, 324-35.
3. Peskin, A. V., Low, F. M., Paton, L. N., Maghzal, G. J., Hampton, M. B. & Winterbourn, C. C. (2007) The high reactivity of peroxiredoxin 2 with H(2)O(2) is not reflected in its reaction with other oxidants and thiol reagents, *J Biol Chem.* **282**, 11885-92.

4. Manta, B., Hugo, M., Ortiz, C., Ferrer-Sueta, G., Trujillo, M. & Denicola, A. (2009) The peroxidase and peroxynitrite reductase activity of human erythrocyte peroxiredoxin 2, *Arch Biochem Biophys.* **484**, 146-54.
5. Trujillo, M., Clippe, A., Manta, B., Ferrer-Sueta, G., Smeets, A., Declercq, J. P., Knoops, B. & Radi, R. (2007) Pre-steady state kinetic characterization of human peroxiredoxin 5: taking advantage of Trp84 fluorescence increase upon oxidation, *Arch Biochem Biophys.* **467**, 95-106.
6. Portillo-Ledesma, S., Randall, L. M., Parsonage, D., Dalla Rizza, J., Karplus, P. A., Poole, L. B., Denicola, A. & Ferrer-Sueta, G. (2018) Differential Kinetics of Two-Cysteine Peroxiredoxin Disulfide Formation Reveal a Novel Model for Peroxide Sensing, *Biochemistry.* **57**, 3416-3424.
7. Parsonage, D., Nelson, K. J., Ferrer-Sueta, G., Alley, S., Karplus, P. A., Furdui, C. M. & Poole, L. B. (2015) Dissecting peroxiredoxin catalysis: separating binding, peroxidation, and resolution for a bacterial AhpC, *Biochemistry.* **54**, 1567-75.
8. Ogusucu, R., Rettori, D., Munhoz, D. C., Netto, L. E. & Augusto, O. (2007) Reactions of yeast thioredoxin peroxidases I and II with hydrogen peroxide and peroxynitrite: rate constants by competitive kinetics, *Free Radic Biol Med.* **42**, 326-334.
9. Noguera, M. E., Vazquez, D. S., Ferrer-Sueta, G., Agudelo, W. A., Howard, E., Rasia, R. M., Manta, B., Cousido-Siah, A., Mitschler, A., Podjarny, A. & Santos, J. (2017) Structural variability of E. coli thioredoxin captured in the crystal structures of single-point mutants, *Sci Rep.* **7**, 42343.
10. Pineyro, M. D., Arcari, T., Robello, C., Radi, R. & Trujillo, M. (2011) Tryparedoxin peroxidases from Trypanosoma cruzi: high efficiency in the catalytic elimination of hydrogen peroxide and peroxynitrite, *Arch Biochem Biophys.* **507**, 287-95.
11. Reyes, A. M., Vazquez, D. S., Zeida, A., Hugo, M., Pineyro, M. D., De Armas, M. I., Estrin, D., Radi, R., Santos, J. & Trujillo, M. (2016) PrxQ B from Mycobacterium tuberculosis is a monomeric, thioredoxin-dependent and highly efficient fatty acid hydroperoxide reductase, *Free Radic Biol Med.* **101**, 249-260.
12. Talwar, D., Messens, J. & Dick, T. P. (2020) A role for annexin A2 in scaffolding the peroxiredoxin 2-STAT3 redox relay complex, *Nature communications.* **11**, 4512.
13. Sobotta, M. C., Liou, W., Stocker, S., Talwar, D., Oehler, M., Ruppert, T., Scharf, A. N. & Dick, T. P. (2015) Peroxiredoxin-2 and STAT3 form a redox relay for H2O2 signaling, *Nat Chem Biol.* **11**, 64-70.
14. Stocker, S., Maurer, M., Ruppert, T. & Dick, T. P. (2018) A role for 2-Cys peroxiredoxins in facilitating cytosolic protein thiol oxidation, *Nat Chem Biol.* **14**, 148-155.
15. Villar, S. F., Ferrer-Sueta, G. & Denicola, A. (2023) The multifaceted nature of peroxiredoxins in chemical biology, *Curr Opin Chem Biol.* **76**, 102355.
16. Szajewski, R. P. & Whitesides, G. M. (1980) Rate constants and equilibrium constants for thiol-disulfide interchange reactions involving oxidized glutathione, *J Am Chem Soc.* **102**, 2011-2026.
17. Forman-Kay, J. D., Clore, G. M. & Gronenborn, A. M. (1992) Relationship between electrostatics and redox function in human thioredoxin: characterization of pH titration shifts using two-dimensional homo- and heteronuclear NMR, *Biochemistry.* **31**, 3442-52.
18. Talwar, D. & Dick, T. P. (2022) Chapter 14 - Thiol peroxidase-based redox relays in *Redox Chemistry and Biology of Thiols* (Alvarez, B., Comini, M. A., Salinas, G. & Trujillo, M., eds) pp. 307-320, Academic Press.
19. Espenson, J. H. (1995) *Chemical Kinetics and Reaction Mechanisms*, McGraw-Hill.

20. Kallis, G. B. & Holmgren, A. (1980) Differential reactivity of the functional sulfhydryl groups of cysteine-32 and cysteine-35 present in the reduced form of thioredoxin from Escherichia coli, *J Biol Chem.* **255**, 10261-5.
21. Mossner, E., Huber-Wunderlich, M. & Glockshuber, R. (1998) Characterization of Escherichia coli thioredoxin variants mimicking the active-sites of other thiol/disulfide oxidoreductases, *Protein Sci.* **7**, 1233-44.
22. Nelson, K. J., Day, A. E., Zeng, B. B., King, S. B. & Poole, L. B. (2008) Isotope-coded, iodoacetamide-based reagent to determine individual cysteine pK(a) values by matrix-assisted laser desorption/ionization time-of-flight mass spectrometry, *Anal Biochem.* **375**, 187-95.
23. Li, H., Hanson, C., Fuchs, J. A., Woodward, C. & Thomas, G. J., Jr. (1993) Determination of the pKa values of active-center cysteines, cysteines-32 and -35, in Escherichia coli thioredoxin by Raman spectroscopy, *Biochemistry.* **32**, 5800-8.
24. Riener, C. K., Kada, G. & Gruber, H. J. (2002) Quick measurement of protein sulfhydryls with Ellman's reagent and with 4,4'-dithiodipyridine, *Anal Bioanal Chem.* **373**, 266-76.
25. Chae, H. Z., Kim, H. J., Kang, S. W. & Rhee, S. G. (1999) Characterization of three isoforms of mammalian peroxiredoxin that reduce peroxides in the presence of thioredoxin, *Diabetes Res Clin Pract.* **45**, 101-12.
26. Dalla Rizza, J., Randall, L. M., Santos, J., Ferrer-Sueta, G. & Denicola, A. (2019) Differential parameters between cytosolic 2-Cys peroxiredoxins, PRDX1 and PRDX2, *Protein Sci.* **28**, 191-201.
27. Villar, S. F., Dalla-Rizza, J., Moller, M. N., Ferrer-Sueta, G., Malacrida, L., Jameson, D. M. & Denicola, A. (2022) Fluorescence Lifetime Phasor Analysis of the Decamer-Dimer Equilibrium of Human Peroxiredoxin 1, *Int J Mol Sci.* **23**, 5620.
28. Bolduc, J. A., Nelson, K. J., Haynes, A. C., Lee, J., Reisz, J. A., Graff, A. H., Clodfelter, J. E., Parsonage, D., Poole, L. B., Furdui, C. M. & Lowther, W. T. (2018) Novel hyperoxidation resistance motifs in 2-Cys peroxiredoxins, *J Biol Chem.* **293**, 11901-11912.
29. Cho, K. J., Park, Y., Khan, T., Lee, J.-H., Kim, S., Seok, J. H., Chung, Y. B., Cho, A. E., Choi, Y., Chang, T.-S. & Kim, K. H. (2015) Crystal Structure of Dimeric Human Peroxiredoxin-1 C83S Mutant, *Bull Korean Chem Soc.* **36**, 1543-1545.
30. Roos, G., Garcia-Pino, A., Van Belle, K., Brosens, E., Wahni, K., Vandenbussche, G., Wyns, L., Loris, R. & Messens, J. (2007) The conserved active site proline determines the reducing power of Staphylococcus aureus thioredoxin, *J Mol Biol.* **368**, 800-11.
31. Singh, R. & Whitesides, G. M. (1990) Comparisons of rate constants for thiolate-disulfide interchange in water and in polar aprotic solvents using dynamic proton NMR line shape analysis, *J Am Chem Soc.* **112**, 1190-1197.
32. Ferrer-Sueta, G. (2022) Chapter 2 - Chemical basis of cysteine reactivity and specificity: Acidity and nucleophilicity in *Redox Chemistry and Biology of Thiols* (Alvarez, B., Comini, M. A., Salinas, G. & Trujillo, M., eds) pp. 19-58, Academic Press.
33. Langford, T. F., Deen, W. M. & Sikes, H. D. (2018) A mathematical analysis of Prx2-STAT3 disulfide exchange rate constants for a bimolecular reaction mechanism, *Free Radic Biol Med.* **120**, 239-245.
34. van Dam, L., Pages-Gallego, M., Polderman, P. E., van Es, R. M., Burgering, B. M. T., Vos, H. R. & Dansen, T. B. (2021) The Human 2-Cys Peroxiredoxins form Widespread, Cysteine-Dependent- and Isoform-Specific Protein-Protein Interactions, *Antioxidants.* **10**, 627.
35. Grassetti, D. R. & Murray, J. F., Jr. (1967) Determination of sulfhydryl groups with 2,2'- or 4,4'-dithiodipyridine, *Arch Biochem Biophys.* **119**, 41-9.

36. Engelman, R., Weisman-Shomer, P., Ziv, T., Xu, J., Arner, E. S. & Benhar, M. (2013) Multilevel regulation of 2-Cys peroxiredoxin reaction cycle by S-nitrosylation, *J Biol Chem.* **288**, 11312-24.
37. Haynes, A. C., Qian, J., Reisz, J. A., Furdui, C. M. & Lowther, W. T. (2013) Molecular basis for the resistance of human mitochondrial 2-Cys peroxiredoxin 3 to hyperoxidation, *J Biol Chem.* **288**, 29714-23.
38. Santos, J., Marino-Buslje, C., Kleinman, C., Ermacora, M. R. & Delfino, J. M. (2007) Consolidation of the thioredoxin fold by peptide recognition: interaction between E. coli thioredoxin fragments 1-93 and 94-108, *Biochemistry.* **46**, 5148-59.
39. Corrales-González, L. (2021) *Cinética de la reducción de peroxirredoxina 1 humana por tiorredoxinas diversas*, Universidad de la República, Montevideo, Uruguay.
40. Carvalho, L. A. C., Truzzi, D. R., Fallani, T. S., Alves, S. V., Toledo, J. C., Jr., Augusto, O., Netto, L. E. S. & Meotti, F. C. (2017) Urate hydroperoxide oxidizes human peroxiredoxin 1 and peroxiredoxin 2, *J Biol Chem.* **292**, 8705-8715.
41. Tairum, C. A., Santos, M. C., Breyer, C. A., Geyer, R. R., Nieves, C. J., Portillo-Ledesma, S., Ferrer-Sueta, G., Toledo, J. C., Jr., Toyama, M. H., Augusto, O., Netto, L. E. & de Oliveira, M. A. (2016) Catalytic Thr or Ser Residue Modulates Structural Switches in 2-Cys Peroxiredoxin by Distinct Mechanisms, *Sci Rep.* **6**, 33133.
42. Ellis, K. J. & Morrison, J. F. (1982) Buffers of constant ionic strength for studying pH-dependent processes, *Methods Enzymol.* **87**, 405-26.
43. Portillo-Ledesma, S., Sardi, F., Manta, B., Tourn, M. V., Clippe, A., Knoops, B., Alvarez, B., Coitino, E. L. & Ferrer-Sueta, G. (2014) Deconstructing the catalytic efficiency of peroxiredoxin-5 peroxidatic cysteine, *Biochemistry.* **53**, 6113-25.
44. Honorato, R. V., Koukos, P. I., Jimenez-Garcia, B., Tsaregorodtsev, A., Verlato, M., Giachetti, A., Rosato, A. & Bonvin, A. (2021) Structural Biology in the Clouds: The WeNMR-EOSC Ecosystem, *Front Mol Biosci.* **8**, 729513.
45. van Zundert, G. C. P., Rodrigues, J., Trellet, M., Schmitz, C., Kastritis, P. L., Karaca, E., Melquiond, A. S. J., van Dijk, M., de Vries, S. J. & Bonvin, A. (2016) The HADDOCK2.2 Web Server: User-Friendly Integrative Modeling of Biomolecular Complexes, *J Mol Biol.* **428**, 720-725.
46. Li, Y., Hu, Y., Zhang, X., Xu, H., Lescop, E., Xia, B. & Jin, C. (2007) Conformational fluctuations coupled to the thiol-disulfide transfer between thioredoxin and arsenate reductase in Bacillus subtilis, *J Biol Chem.* **282**, 11078-83.
47. Chartron, J., Shiau, C., Stout, C. D. & Carroll, K. S. (2007) 3'-Phosphoadenosine-5'-phosphosulfate reductase in complex with thioredoxin: a structural snapshot in the catalytic cycle, *Biochemistry.* **46**, 3942-51.
48. Ma, X. X., Guo, P. C., Shi, W. W., Luo, M., Tan, X. F., Chen, Y. & Zhou, C. Z. (2011) Structural plasticity of the thioredoxin recognition site of yeast methionine S-sulfoxide reductase Mxr1, *J Biol Chem.* **286**, 13430-7.
49. Hwang, J., Suh, H. W., Jeon, Y. H., Hwang, E., Nguyen, L. T., Yeom, J., Lee, S. G., Lee, C., Kim, K. J., Kang, B. S., Jeong, J. O., Oh, T. K., Choi, I., Lee, J. O. & Kim, M. H. (2014) The structural basis for the negative regulation of thioredoxin by thioredoxin-interacting protein, *Nature communications.* **5**, 2958.
50. Maier, J. A., Martinez, C., Kasavajhala, K., Wickstrom, L., Hauser, K. E. & Simmerling, C. (2015) ff14SB: Improving the Accuracy of Protein Side Chain and Backbone Parameters from ff99SB, *J Chem Theory Comput.* **11**, 3696-713.

51. Pedron, F. N., Messias, A., Zeida, A., Roitberg, A. E. & Estrin, D. A. (2023) Novel Lennard-Jones Parameters for Cysteine and Selenocysteine in the AMBER Force Field, *J Chem Inf Model*. **63**, 595-604.
52. D.A. Case, I.Y. Ben-Shalom, S.R. Brozell, D.S. Cerutti, T.E. Cheatham, I., V.W.D. Cruzeiro, T.A. Darden, R.E. Duke, D. Ghoreishi, M.K. Gilson, H. Gohlke, A.W. Goetz, D. Greene, R Harris, N. Homeyer, Y. Huang, S. Izadi, A. Kovalenko, T. Kurtzman, T.S. Lee, S. LeGrand, P. Li, C. Lin, J. Liu, T. Luchko, R. Luo, D.J. Mermelstein, K.M. Merz, Y. Miao, G. Monard, C. Nguyen, H. Nguyen, I. Omelyan, A. Onufriev, F. Pan, R. Qi, D.R. Roe, A. Roitberg, C. Sagui, S. Schott-Verdugo, J. Shen, C.L. Simmerling, J. Smith, R. SalomonFerrer, J. Swails, R.C. Walker, J. Wang, H. Wei, R.M. Wolf, X. Wu, L. Xiao, York, D. M. & Kollman, P. A. (2018) AMBER 2018, University of California, San Francisco in
53. Rastelli, G., Del Rio, A., Degliesposti, G. & Sgobba, M. (2010) Fast and accurate predictions of binding free energies using MM-PBSA and MM-GBSA, *J Comput Chem.* **31**, 797-810.

Table 1. Second order rate constants of the reduction of $PrxS_2$ by $Trx(SH)_2$ and TCEP. Values obtained from Figs. 2 and 3. In parentheses are the interpreted position of each rate constant in the catalytic cycle of Fig. 1. This interpretation is found in the Results and Discussion section.

Reductant	Prx1	Prx2
	k (M^{-1} s^{-1})	
TCEP	3.66	6.25
*Hs*Trx1	$k_{up} = 2.2 \pm 0.1 \times 10^6$ (k_{3a}) $k_{dn} = 15.8$ s^{-1} (k_{3b}, k_{3c} or k_{3d})	$k_{dn} = 6.1 \pm 0.2 \times 10^5$ (k_{3a} or k_{3ab}^{pe}) $k_{up} = 0.17$ s^{-1} (k_2)
*Hs*Trx2	$k_{up} = 1.9 \pm 0.02 \times 10^6$ (k_{3a}) $k_{dn} = 40.9$ s^{-1} (k_{3b}, k_{3c} or k_{3d})	$k_{dn} = 5.2 \pm 0.1 \times 10^5$ (k_{3a} or k_{3ab}^{pe}) $k_{up} = 0.17$ s^{-1} (k_2)
*Ec*Trx	$k_{up} = 2.5 \pm 0.6 \times 10^6$ (k_{3a}) $k_{dn} = 5.3 \pm 0.6 \times 10^5$ (k_{3ab}^{pe})	$k_{dn} = 4.2 \pm 0.2 \times 10^5$ (k_{3a} or k_{3ab}^{pe}) $k_{up} = 0.21$ s^{-1} (k_2)

Table 2. pK_a values of the nucleophilic cysteine of Trx measured by their reaction with $Prx2S_2$, compared to other means with free Trx.

Trx	pK_a		
	Prx2 reduction	Chemical reaction/Spectroscopic	Literature values
*Hs*Trx1	5.3 ± 0.18	6.1 ± 0.14 and 7.6 ± 0.14 (oxidation with 4-DTDPy)	6.3 [17]
*Hs*Trx2	5.9 ± 0.24	6.5 ± 0.09 (UV absorption) 7.1 ± 0.05 (oxidation with 4-DTDPy)	
*Ec*Trx	6.2 ± 0.2	7.4 ± 0.11 (oxidation with 4-DTDPy)	6.7 [20] 7.2 – 7.5 [9] 7.1 – 7.4 [21] 6.5 [22] 7.1 [23]

Figure legends

Figure 1. Extended canonic catalytic cycle of a 2-Cys Prx. The numbers indicate the sequence of reactions: 1 Oxidation by H_2O_2, 2 Resolution, and 3 Reduction by Trx. The Reduction step is subdivided in 3a Prx-Trx non covalent association, 3b first thiol-disulfide exchange, 3c second thiol-disulfide exchange, and 3d dissociation of the Prx-Trx non covalent complex. The "fully folded" (*FF*) and "locally unfolded" (*LU*) states are indicated.

Figure 2. A. Scheme of the rate-limiting approach. **B.** Time courses of reduction of 4 μM $Prx2S_2$ by 0.2 μM $Trx(SH)_2$ in the presence of 1 μM H_2O_2. The lines are averages of ten runs with *Hs*Trx1 (●), *Hs*Trx2 (■), or *Ec*Trx (▲), and the gray line is a control experiment without Trx. The best fit to equation 2 yields two rate constants: one for the descending part of the time courses (k_{dn}, **C**) and one for the ascending part (k_{up}, **D**). Best fit slopes of panel **C** and *y*-intercepts of panel **D** are in Table 1.

Figure 3. Reduction of Prx1 by Trx. A, B and C. Time courses of reduction of $Prx1S_2$ with 45.6 μM *Hs*Trx1, 54 μM *Hs*Trx2, or 40 μM *Ec*Trx, respectively. **D.** Second-order plot of the ascending exponential rate constant (k_{up}) vs [*Hs*Trx1] (■), [*Hs*Trx2] (●) or [*Ec*Trx] (▲), slopes of the linear regressions, $2.2 \pm 0.5 \times 10^6$, $1.9 \pm 0.02 \times 10^6$, $2.8 \pm 0.7 \times 10^6$ M^{-1} s^{-1}, respectively. **E.** Second-order plot of the descending exponential rate constant (k_{dn}) vs [*Hs*Trx1] (■), [*Hs*Trx2] (●) or [*Ec*Trx] (▲), slopes of the linear regressions, 0, 0 and $5.3 \pm 0.6 \times 10^5$ M^{-1} s^{-1} respectively. The former two horizontal lines were forced in the regression, see text.

Figure 4. Reduction of Prx2 by Trx as a function of pH and comparison with DTDPy. Panels **A**, **B** and **C** show reaction time courses at selected pH values for *Hs*Trx1, *Hs*Trx2 and *Ec*Trx, respectively. **D.** The rate constant of the descent in fluorescent emission plotted vs pH has a bell-shaped profile that can be described by a two pK_a function (Equation 4). Best fit values of pK_a are: 5.6 and 7.2 for *Hs*Trx1, 6.1 and 7.7 for *Hs*Trx2, and 6.4 and > 8.5 for *Ec*Trx. **E.** Oxidation of each Trx by DTDPy in excess, as a function of pH, has inflection points consistent with the C_N of the free protein having pK_a = 6.1 and 7.6 (*Hs*Trx1), 7.1 (*Hs*Trx2), and 7.4 (*Ec*Trx).

Figure 5. Features of Prx2-Trx interaction. A. Cartoon representation of the predicted complex between $Prx2S_2$ (blue) and *Hs*Trx1 (orange). The interaction area is shown as a surface, where regions 1 (gray) and 2 (green) are depicted. **B.** MM-GBSA $\Delta G_{Binding}$ estimation (kcal/mol) for each complex **C.** Decomposition of the $\Delta G_{Binding}$ in a per residue basis for *Hs*Trx1. Most relevant residues at the interaction surface are shown for *Hs*Trx1 (**D**), *Hs*Trx2 (**E**) and *Ec*Trx (**F**). Regions 1 and 2 are represented as surfaces and the residues are depicted as blue ($Prx2(S)_2$), orange (*Hs*Trx1), magenta (*Hs*Trx2) and red (*Ec*Trx) sticks.

Figure 6. Effect of C_N protonation on Prx2-Trx interaction. Per residue decomposition of the $\Delta G_{Binding}$ of the Prx2-Trx complex, for **A** *Hs*Trx1, **B** *Hs*Trx2, and **C** *Ec*Trx, in all cases C_NSH (gray) and C_NS^- (red) are compared. The insets represent the overall $\Delta G_{Binding}$. Residue names colored according to each Trx and blue tohes of Prx2. **D.** Time courses of W31 dihedral (black) and $\Delta G_{Binding}$ (blue) values against the simulated time. The red-dashed lines indicate the time correspondence of the "jumps" in the properties. **E.** Ball and stick representation of W31 and C32 at the indicated W31 dihedral values. **F.** Normalized relative frequency of *Hs*Trx1 W31 C-Cα-Cβ-Cγ dihedral throughout the simulation for C_NSH and C_NS^-. The $\Delta G_{Binding}$ of the complex at values -80°, -50° and 60° is represented as blue circles. *Error bars represent the standard deviation of the obtained values.

Figure 7. The Prx2-Trx complex shields C_NS^- from the solvent. A. Violin plot of the distribution of water molecules within 5 Å of C_N sulfur atom during the simulated time. C_NSH, C_NS^- and C_NS^- without Prx2 are compared. **B.** Radial pair distribution function (g(r)) of water around C_N sulfur for the three situations. **C.** Structural representation of the water molecules surrounding C_N sulfur. W31, C_N and the Prx2 disulfide are represented as sticks (behind the transparent surface), while water molecules are depicted as ball and stick. Surface colors orange and blue represent *Hs*Trx1 and Prx2, respectively.

Figure 1

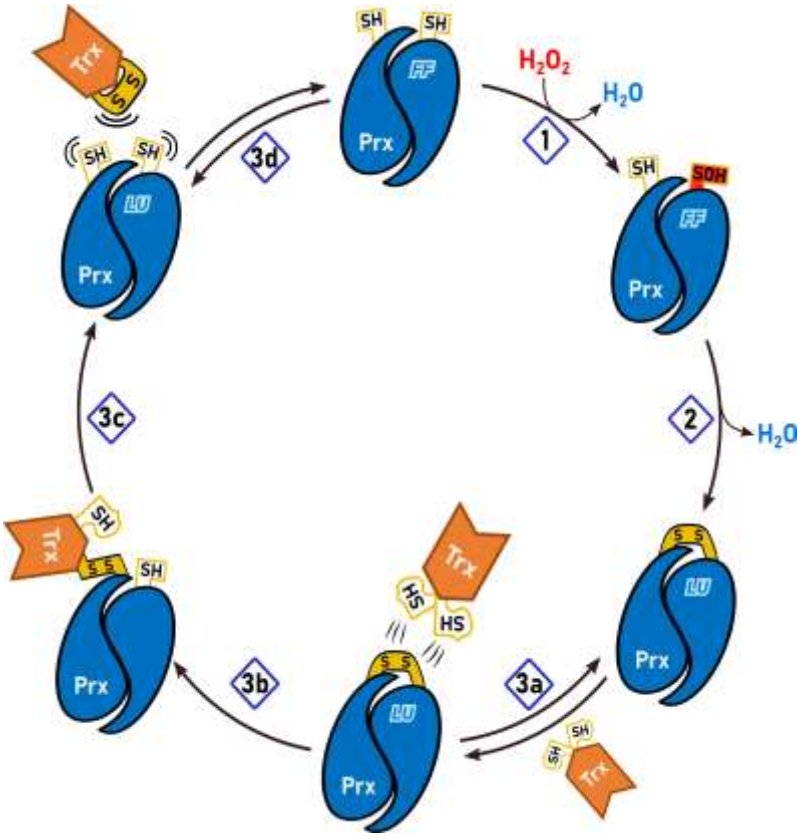

Figure 2

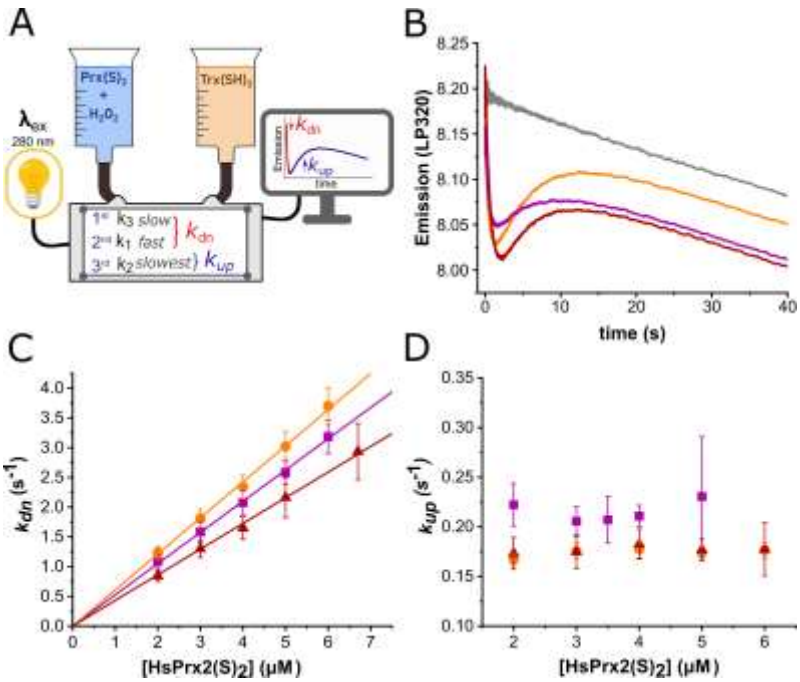
A
B
C
D
Prx(S)2 + H2O2
Trx(SH)2
λexc 280 nm
1st k3 slow
2nd k1 fast
3rd k2 slowest
kdn
kup
Emission
time
Emission (LP320)
time (s)
kdn (s-1)
[HsPrx2(S)2] (μM)
kup (s-1)
[HsPrx2(S)2] (μM)

Figure 3

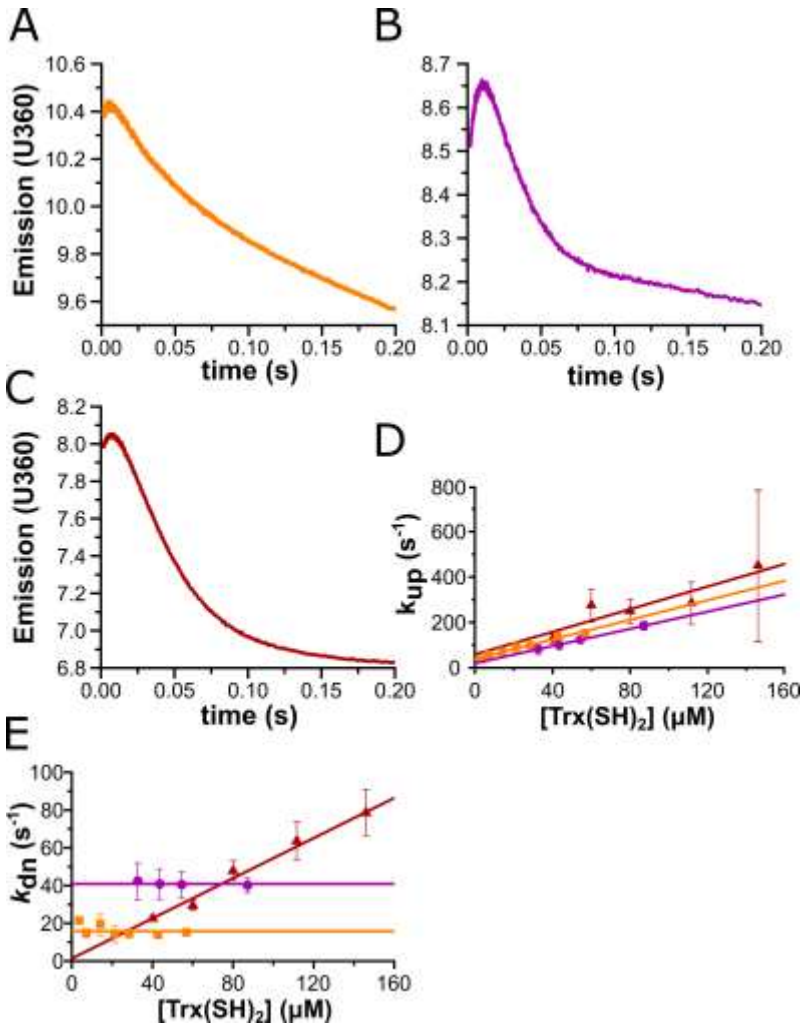

Figure 4

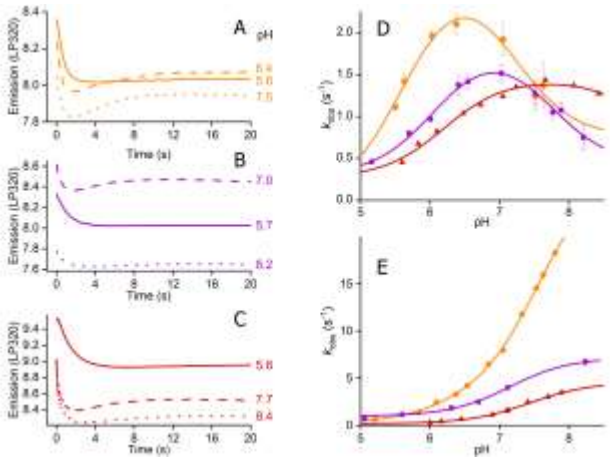
A
pH
Emission (LP320)
Time (s)
B
Emission (LP320)
Time (s)
C
Emission (LP320)
Time (s)
D
pH
E
pH

Figure 5

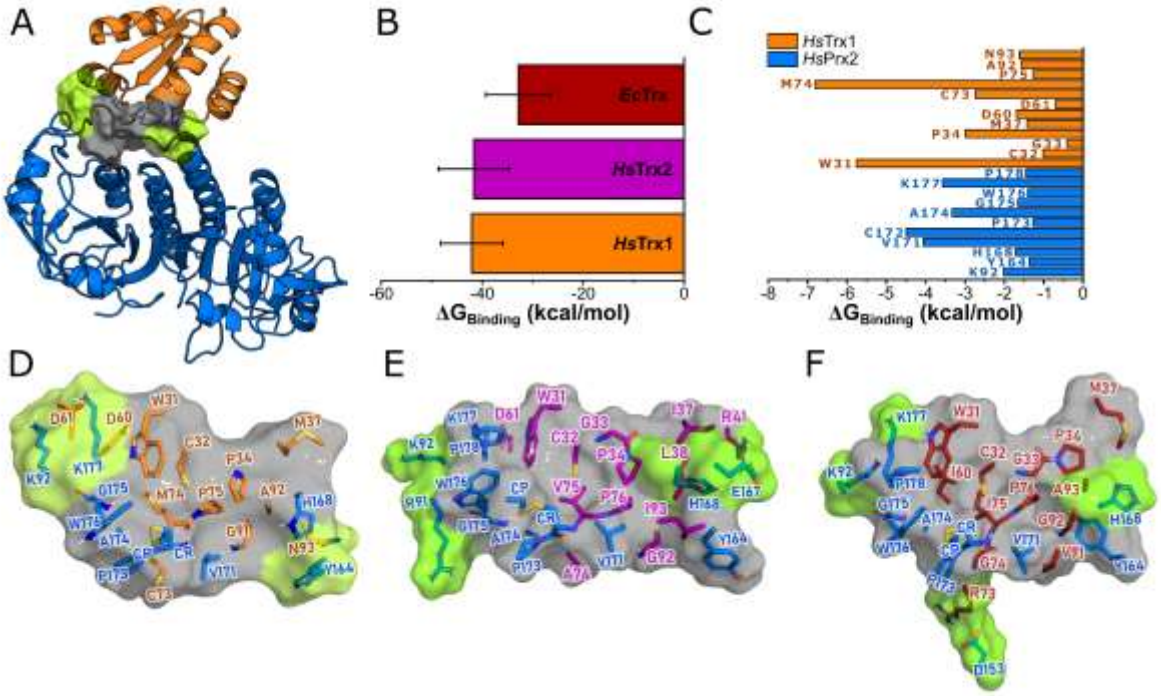
A
B
C
EcTrx
HsTrx2
HsTrx1
-60
-40
-20
0
ΔG Binding (kcal/mol)
HsTrx1
HsPrx2
M74
C73
P34
W31
K177
A174
C172
V171
K92
-8
-7
-6
-5
-4
-3
-2
-1
0
ΔG Binding (kcal/mol)
D
E
F

Figure 6

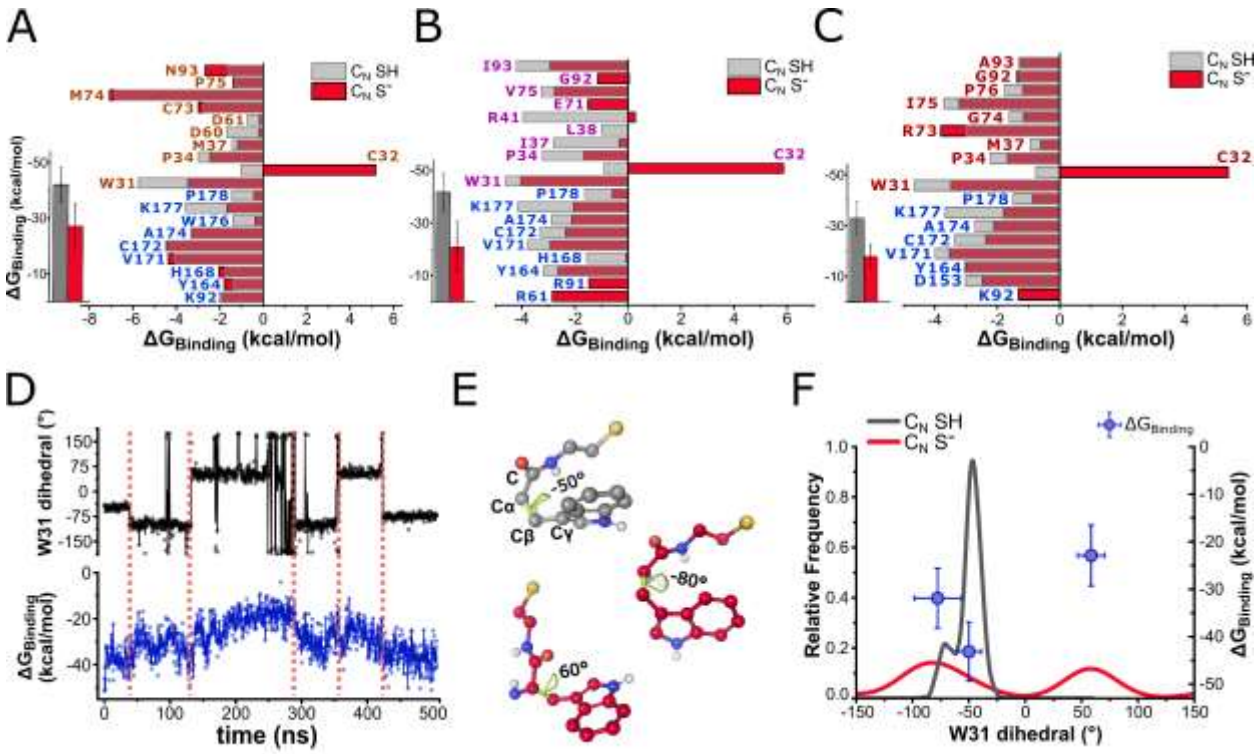
A
B
C
D
E
F
C_N SH
C_N S$^-$
$\Delta G_{Binding}$ (kcal/mol)
W31 dihedral (°)
time (ns)
Relative Frequency
W31 dihedral (°)
$\Delta G_{Binding}$
-50°
-80°
60°

Figure 7

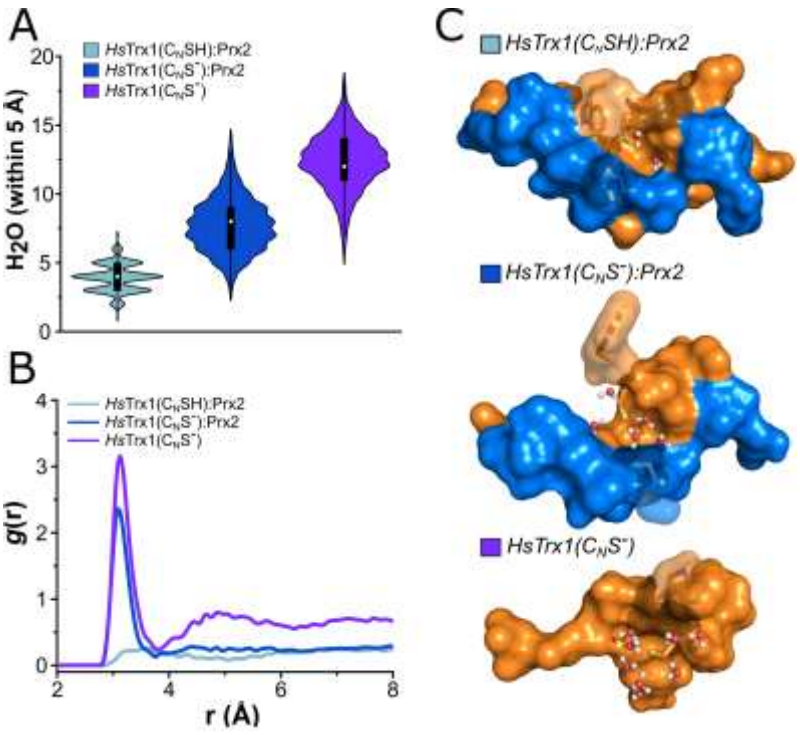
A
HsTrx1(CNSH):Prx2
HsTrx1(CNS⁻):Prx2
HsTrx1(CNS⁻)
H2O (within 5 Å)
20
15
10
5
0
B
HsTrx1(CNSH):Prx2
HsTrx1(CNS⁻):Prx2
HsTrx1(CNS⁻)
g(r)
4
3
2
1
0
2
4
6
8
r (Å)
C
HsTrx1(CNSH):Prx2
HsTrx1(CNS⁻):Prx2
HsTrx1(CNS⁻)